Formation and evolution of high plasma pressure region in the near-Earth plasma sheet: Pre-cursor and post-cursor of substorm expansion onset

AUTHOR(S):

Yao, Y.; Ebihara, Y.; Tanaka, T.

CITATION:

Yao, Y. ...[et al]. Formation and evolution of high plasma pressure region in the near-Earth plasma sheet: Pre-cursor and post-cursor of substorm expansion onset. Journal of Geophysical Research 2015, 120(8): 6427-6435

ISSUE DATE:

2015-08

URL:

http://hdl.handle.net/2433/237234

AGU PUBLICATIONS
JGR
Journal of Geophysical Research: Space Physics

RESEARCH ARTICLE
10.1002/2015JA021187

Key Points:
- High-pressure region moves earthward before onset and tailward after onset
- Flow convergence is responsible for evolution of the high-pressure region
- MHD simulation is consistent with THEMIS observation on substorm sequence

Supporting Information:
- Texts S1 and S2 and Figures S1–S4

Correspondence to:
Y. Yao,
yyao0103@gmail.com

Citation:
Yao, Y., Y. Ebihara, and T. Tanaka (2015), Formation and evolution of high-plasma-pressure region in the near-Earth plasma sheet: Precursor and postcursor of substorm expansion onset, *J. Geophys. Res. Space Physics*, *120*, 6427–6435, doi:10.1002/2015JA021187.

Received 4 MAR 2015
Accepted 26 JUL 2015
Accepted article online 29 JUL 2015
Published online 20 AUG 2015
Corrected 17 NOV 2015

This article was corrected on 17 NOV 2015. See the end of the full text for details.

Formation and evolution of high-plasma-pressure region in the near-Earth plasma sheet: Precursor and postcursor of substorm expansion onset

Y. Yao[1], Y. Ebihara[1], and T. Tanaka[2]

[1]Research Institute for Sustainable Humanosphere, Kyoto University, Uji, Japan, [2]Kyushu University, Fukuoka, Japan

Abstract Cause of substorm expansion onset is one of the major problems in the magnetospheric study. On the basis of a global magnetohydrodynamic (MHD) simulation, Tanaka et al. (2010) suggested that formation and evolution of a high-pressure region (HPR) in the near-Earth plasma sheet could result in sudden intensification of the Region 1 field-aligned current and the westward auroral electrojet. In this sense, the formation and evolution of the HPR are a key in understanding the cause of the onset. On 5 April 2009, three probes of the Time History of Events and Macroscale Interactions during Substorms (THEMIS) were located at X_{GSM}~−11 *Re* around the equator, which provide unique opportunity to investigate the spatial-temporal evolution of the HPR near the substorm expansion onset. Just before the onset, a positive excursion of the plasma pressure appeared at the outermost probe first, followed by the inner ones. Just after the onset, the opposite sequence took place. A positive excursion of the *Y* component of the current density was observed near the onset by the THEMIS probes and followed by a decrease trend. A similar variation was also found in the MHD simulation. All these features are consistent with the simulation result that a squeeze of the plasma from the plasma sheet results in the formation of the HPR before the onset and that the accumulated plasma spreads outward after the onset. The HPR is shown to be important for the dynamics of the magnetosphere during a substorm.

1. Introduction

Substorm is a transient phenomenon, during which the solar wind energy is transferred into magnetic energy stored in the magnetotail, and then significantly released into the inner magnetosphere, and the ionosphere. The time of a sudden brightening of the aurora [*Akasofu*, 1964] is widely accepted as a substorm expansion onset. The key issue in the substorm is its triggering mechanism. Numerous models have been proposed, such as the near-Earth neutral line (NENL) model [e.g., *Baker et al*., 1996], in which the onset is triggered by the process of magnetic reconnection at ~20 *Re* in the near-Earth magnetotail, and the current disruption (CD) model [e.g., *Lui*, 1996], in which the ballooning instability or cross-field current instability causes the CD at ~10 *Re*, resulting in the dipolarization and formation of the substorm current wedges. A synthesis of the models have also been suggested [*Pu et al*., 1999; *Machida et al*., 2014].

On the basis of a global magnetohydrodynamic (MHD) simulation, *Tanaka et al*. [2010] pointed out that the sudden intensification of the westward auroral electrojet can be explained in terms of a substantial increase of the plasma pressure caused by the state transition (change in the force balance) in the plasma sheet. The state transition model involves the MHD processes only. During the growth phase, about 6 min before the substorm expansion onset a near-Earth neutral line (NENL) forms and results in the force imbalance between pressure gradient force and tension force. It is always over tension in the midtail region just before the onset, since the reduction of the pressure gradient force. The over tension state brings out earthward tension force that generates earthward fast flow. The convergence of the fast flow contributes to the pressure enhancement that leads to the generation of high-pressure region (HPR). In other words, the plasma is squeezed in the near-Earth plasma sheet resulting in the formation of high-pressure region. Also, it can be said that the plasma implodes earthward. As a consequence, the HPR moves earthward and reaches the inner region from $X_{GSM} = -6$ to -8 *Re* within 3 or 4 min before the onset. The generation of the HPR causes diamagnetic current (J_d) that can result in an intensification of the Region 2 field-aligned currents, together with the Region 1 currents on the nightside. Then, auroral electrojets are intensified in the polar ionosphere on the nightside, which is regarded as a manifestation of the substorm expansion onset. After the onset, the region where

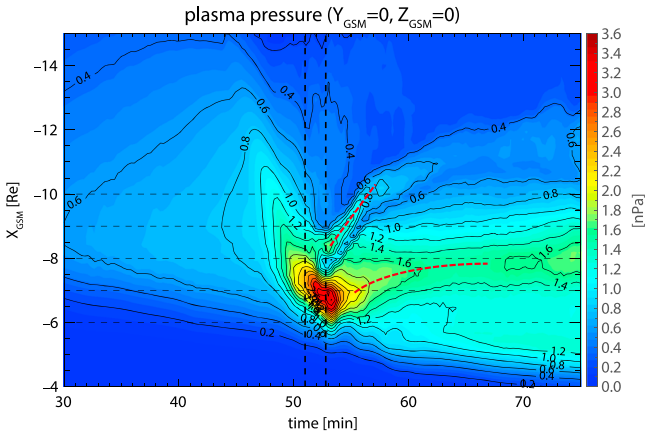

Figure 1. Temporal variation of simulated plasma pressure as a function of X_{GSM} in the equatorial plane ($Y_{GSM} = 0$ and $Z_{GSM} = 0$ *Re*). The vertical dashed lines refer to the time at elapsed times of 51 and 52.8 min. The horizontal lines give reference from $X_{GSM} = -6$ to -10 *Re* with 1 *Re* interval. The red thick curve and line indicate evolution of the main part and sub part of the high-pressure region after the substorm onset, respectively.

the plasma is squeezed spreads tailward. As a consequence, the HPR retreats tailward, although the plasma flows earthward. *Yao et al.* [2015] identified the tailward propagation of the HPR just after the onset that took place on 1 March 2008 on the basis of data from the Time History of Events and Macroscale Interactions during Substorms (THEMIS) probes. However, the earthward implosion of the HPR before the onset as predicted by the global MHD simulation was not identified. One possible reason is that the THEMIS probes were located at off-equator during the substorm on 1 March 2008. The purpose of this study is to identify the earthward implosion and tailward retreat of the HPR before and after the onset, respectively, and associate the propagation of the HPR with a substorm expansion onset in terms of precursor and postcursor of the onset.

2. Observations and MHD Simulation Results

We used the global MHD simulation developed by *Tanaka et al.* [2010]. The boundary condition in the upstream of the solar wind is the same as the one used by *Ebihara and Tanaka* [2013] and *Yao et al.* [2015], solar wind speed of 372.4 km/s, solar wind density of 10 cm^{-3}, and interplanetary magnetic field (IMF) B_y of 4.33 nT and B_z of -4.33 nT. Figure 1 shows the plasma pressure calculated by the global MHD simulation as a function of X_{GSM} and time in equatorial plane ($Z_{GSM} = Y_{GSM} = 0$ *Re*). Elapsed time at 51 min (in which the epoch starts with the southward turning of IMF) is defined as a plausible substorm onset based on a sharp slope of the *AL* index [*Ebihara and Tanaka*, 2013]. The near-Earth neutral line (NENL) is formed at X_{GSM}~-15 *Re* at elapsed time of ~45 min. After the formation of the NENL, it is found that the plasma pressure starts to increase in the outer region first, followed by the inner region. The HPR seems to implode earthward. When the HPR arrives at $X_{GSM} = -7$ *Re*, a substorm expansion onset takes place. After the onset, the HPR splits into two. A main part (inner part) of the HPR continues to move earthward between 51 and 53 min, and then after ~53 min, it begins to expand both earthward and tailward. After ~52.8 min, a subpart (outer part) of the HPR could be seen on the outer side of the main one between $X_{GSM} = -8$ and -9 *Re*. The subpart only retreats tailward. The main part of the HPR results from the convergence of the thermal energy, and the subpart of the HPR comes from the flow braking [*Tanaka et al.*, 2010]. The "V" structure that appears in the X_{GSM}-time diagram of the plasma pressure is a characteristic feature seen in the global MHD simulation [*Tanaka et al.*, 2010].

On 5 April 2009, an isolated substorm occurred during the interval that *Dst* index was 4 nT. According to the SuperMAG database [*Gjerloev*, 2012], the substorm expansion onset took place at ~09:17 UT based on a sharp decrease in the auroral electrojet index (*SML*) of the SuperMAG. *AL* index provided by WDC Kyoto reached -217 nT, so that this substorm may be regarded as a weak one. During the period from 09:10 to 09:30 UT (including both substorm growth and expansion phases), the average solar wind conditions are as follows: solar wind density of 7.13 cm^{-3}, solar wind speed of 347.26 km/s, IMF B_y of 2.82 nT, and B_z of -1.31 nT. In this substorm event, three THEMIS [*Angelopoulos*, 2008] probes THA, THD, and THE were distributed close to each other at X_{GSM} = ~-11 *Re*. The locations of the probes are shown in Figure 2 by solid circles as its start position. Solid lines indicate their orbits during the period between 09:00 and 10:00 UT. Figure 2b shows the locations of the probes in the X_{GSM}-Z_{GSM} plane, together with magnetic field lines provided by the T89-magnetic field model [*Tsyganenko*, 1989]. Probe THE was located at (-11.1, 2.3, 0.0) *Re*, and probe THD was located at (-10.7, 1.2, 0.3) *Re* in the GSM coordinate, so that these two probes were located very close to the equatorial

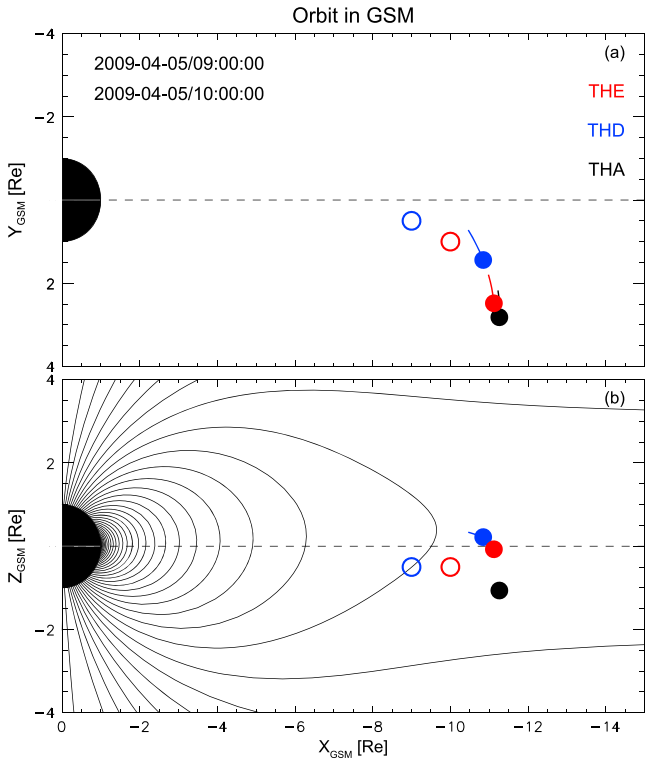

Figure 2. Orbit of THEMIS probes (THD, THE, and THA) shown by solid circle (start point) with line pointing the orbit in (a) X_{GSM}-Y_{GSM} and (b) X_{GSM}-Z_{GSM} planes during the period between 09:00 and 10:00 UT on 5 April 2009. The open circles refer to coincident positions of the associated THEMIS probes in the MHD simulation domain (see text for details).

plane. Probe THA was located at (−11.3, 2.6, −1.0) *Re*, which occupies the similar Y_{GSM} value as that of probe THE. In this study we used the same method as utilized by *Yao et al.* [2015] to determine the coincident position of the THEMIS probes in the MHD simulation domain. That is, at the coincident position, the overall variations of plasma pressure, bulk velocity, and magnetic field are similar to those observed by a corresponding probe. The coincident positions are drawn by open circles.

Figure 3 demonstrates direct comparison between the THEMIS observation and the MHD simulation at probes THE and THD. Probe THE is about 0.4 *Re* tailward far from probe THD. Figure 3a shows *SML* of the SuperMAG, *AL* index from WDC Kyoto, and THEMIS *AL* index denoted by red, blue, and dark green lines, respectively. According to the SuperMAG database, the substorm expansion onset is determined at ~09:17 UT. Figure 3b shows *AL* index computed from the simulation data [*Ebihara and Tanaka*, 2013]. In the MHD simulation, we define the time of the onset to the moment at which the calculated *AL* starts to decrease rapidly, that is elapsed time of ~51 min [*Ebihara and Tanaka*, 2013]. The determined onset times are indicated by vertical dashed lines in Figures 3a and 3b.

Each THEMIS probe carries two different instruments to detect ions, the electrostatic analyzer (ESA) [*McFadden et al.*, 2008] for ions with energy <25 keV and Solid State Telescope (SST) [*Angelopoulos*, 2008] with energy >30 keV. In this study we defined the ion pressure observed by the THEMIS probes as a combination of the ion pressure from ESA (P_{ESA}) and SST (P_{SST}). Figure 3c shows the observed ion pressure at probe THE. Although the ion pressure shows fluctuations, at least two major peaks can be clearly seen before and after the onset as denoted by horizontal bars. The pressure observed by probe THD, which was located closer to the Earth than probe THE, is shown in Figure 3e. Two peaks can also be found before and after the onset as denoted by horizontal bars. Time difference between two pressure peaks is smaller at probe THD than that at probe THE. Figures 3d and 3f show the plasma pressure obtained by the MHD simulation at the coincident positions of probes E and D, respectively. Two pressure peaks are also seen as denoted by solid triangles, and the time difference between the two pressure peaks is smaller at coincident position of probe THD than that at probe THE. It is plausible to indicate that the THEMIS probes could capture the V structure shown in Figure 1.

Probe THE observed a decrease in the ion pressure from 09:06 UT (out of the time range shown in Figure 3c) and a sharp enhancement from ~09:15 UT. The ion pressure decrease here is due to that probe THE moved away from the central plasma sheet (CPS). From ion energy flux (not shown here), it is obvious that there is a decrease in energy level associated to the ion pressure decrease, which may correspond to the movement of probe THE toward the boundary layer. The ion pressure sharp enhancement from 09:15 UT is the result of encountering the HPR propagating earthward, which is located within the CPS, and partially due to the location change. At ~09:15 UT probe THE moved back to the CPS, and encountered the HPR, which causes the sharp pressure enhancement. The evidence can be found from the ion energy flux that has a similar enhancement pattern as that observed by probe THD that was always located in the CPS, the fast earthward flow that

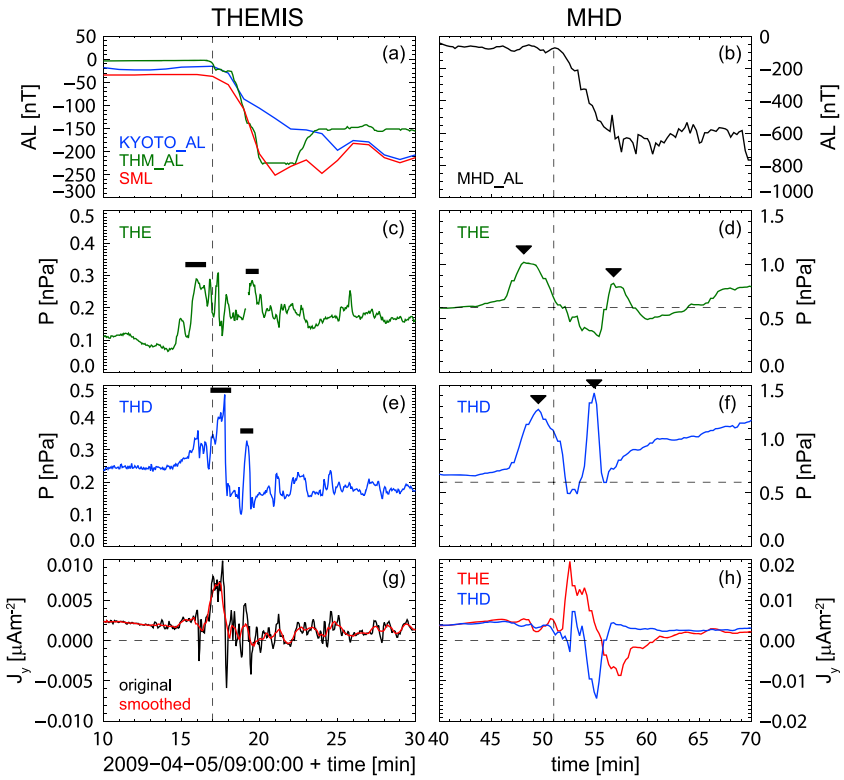

Figure 3. Comparison between THEMIS observations and results of MHD simulation. (a) *SML* of the SuperMAG (red), *AL* index of WDC Kyoto (blue), and THEMIS *AL* index (dark green). (b) *AL* index computed from the simulation data. (c and d) The comparison of plasma pressure between THEMIS observation and simulation at probe THE. (e and f) The comparison of plasma pressure at probe THD. (g) J_y calculated from the observations of THEMIS probes (see text for details). (h) Simulated J_y at coincident position of probes THE (red) and THD (blue) in the MHD frame.

can be seen associated to the HPR earthward propagation. The location change can contribute to the pressure variation since the particle properties are different in the CPS and the boundary layer, but only a glossy enhancement is available.

On the basis of the multispacecraft measurements of the magnetic field obtained by the THEMIS probes, *Lui* [2011] and *Yao et al*. [2014] demonstrated a way to directly calculate the current density in the Y_{GSM} direction by using Ampere's

$$\mu_0 J = \nabla \times B, \tag{1}$$

where μ_0 is the magnetic constant, **J** is the current density, and B is the magnetic field. The current density in the Y-component J_y is thus given by

$$J_y = \frac{1}{\mu_0}\left(\frac{\partial B_x}{\partial z} - \frac{\partial B_z}{\partial x}\right); \quad \frac{1}{\mu_0}\left(\frac{\Delta B_x}{\Delta z} - \frac{\Delta B_z}{\Delta x}\right). \tag{2}$$

In this study, $\Delta B_x/\Delta z$ is calculated by the observed data from a pair of two probes THE and THA, and $\Delta B_z/\Delta x$ is calculated by the data obtained from a pair of two probes THE and THD. We assumed that the magnetic field is independent of Y_{GSM}. Figure 3g shows the J_y calculated based on the THEMIS observations. The black line indicates J_y with a temporal resolution of 3 s. The red line refers to the smoothed one with a 30 s running average window from the original data in black line. A positive excursion of J_y is found near or a little bit after the substorm expansion onset, which is consistent with the global MHD simulation result shown in Figure 3h.

Figure 4 summarizes the plasma pressure P, the plasma velocity V, the magnetic field B, and the current density **J** in the GSM coordinates. All the parameters are obtained from the global MHD simulation at (−10.0, 1.0, −0.5) *Re*, that is the coincident position of probe THE. Two vertical dashed lines from left to right refer to times at elapsed times of 51 (substorm expansion onset) and 55 min, respectively.

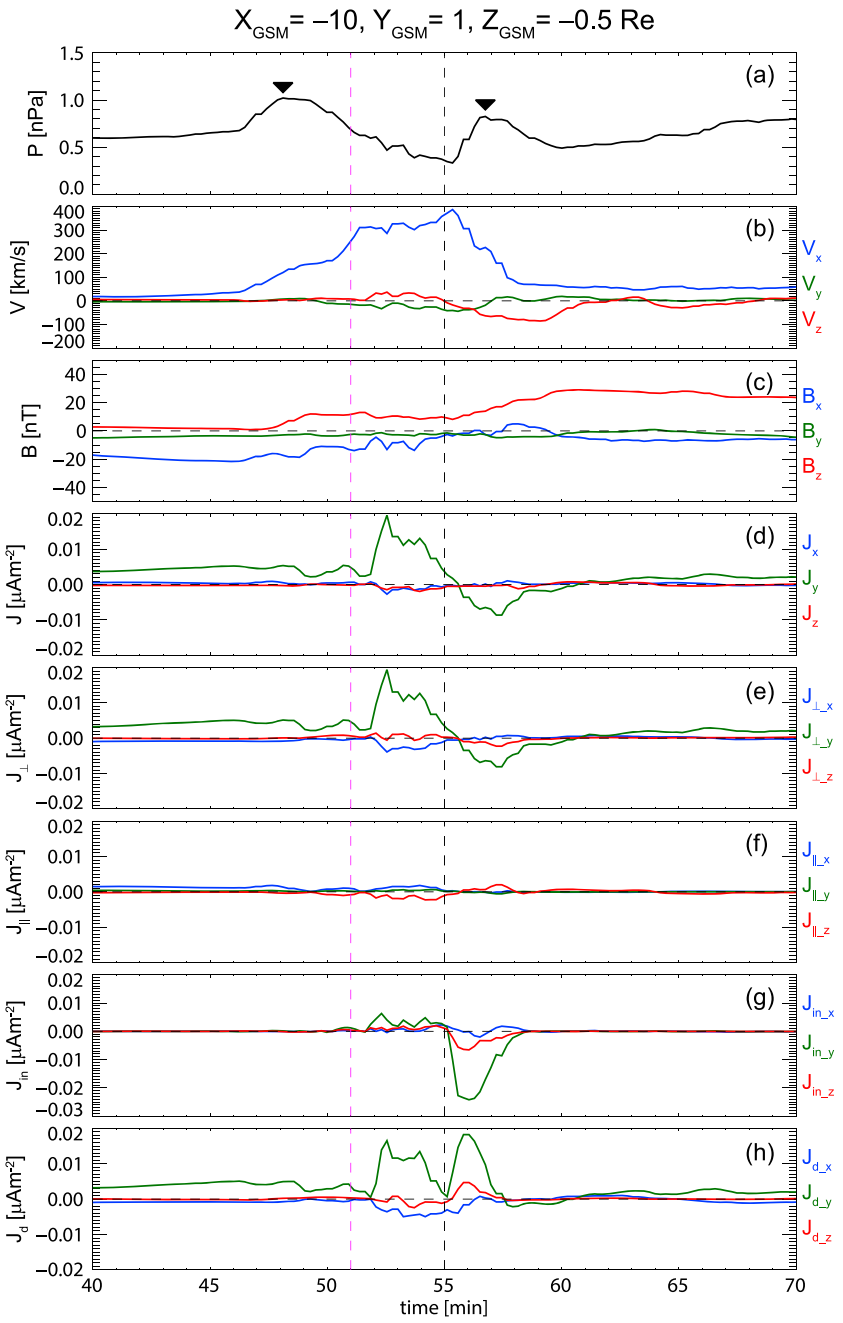

Figure 4. Temporal variation of simulated (a) plasma pressure and (b) velocity in GSM coordinate; the blue, dark green, and red lines refer to V_x, V_y, and V_z, respectively (following vectors have the same format as velocity), (c) magnetic field, (d) current density, (e) perpendicular current density, (f) parallel current density, (g) inertial current density, (h) diamagnetic current density. The two vertical dashed lines indicate the time at 51 and 55 min.

In Figure 4a two pressure peaks can be found as denoted by solid triangles, which are also found in Figure 1. The first one is found before the onset at ~48 min, and the other one is found after the onset around 56 min. Figure 4b shows the plasma velocity *V*. The *X* component of the velocity (V_x) starts to increase at ~46 min. After the onset (~51 min), V_x further increases and reaches maximum at ~55 min. Then, V_x decreases. The magnitude of V_y and V_z is small as compared with that of V_x. After the onset V_z shows a negative excursion around 55 min. This feature is normally found in the tailward retreat of the HPR away from the equator, in which plasma moves away from the equator in the Z_{GSM} direction because of the establishment of the pressure gradient force looking away from the equatorial plane [*Yao et al.*,

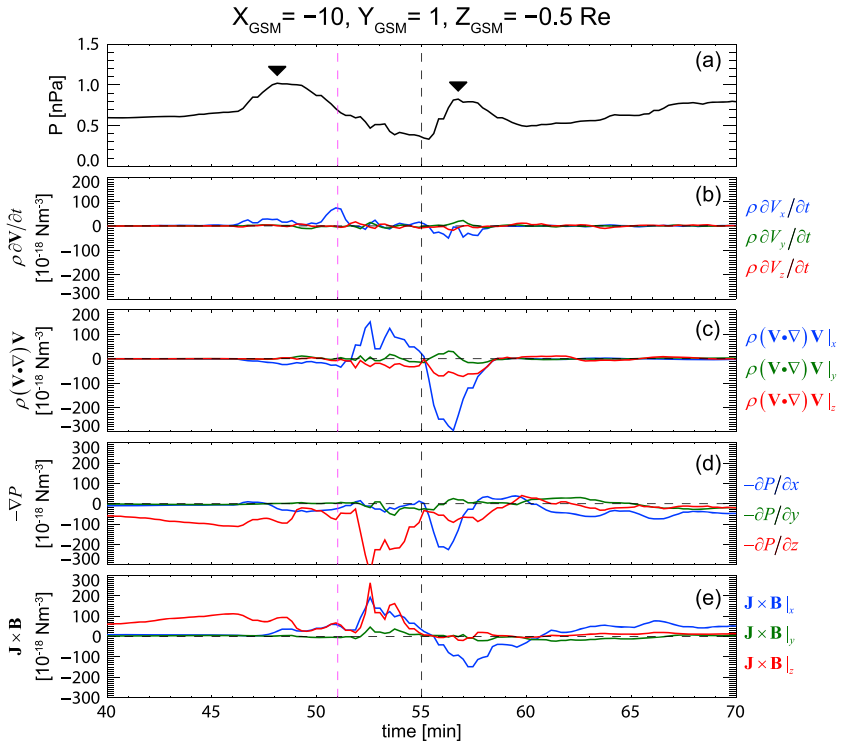

Figure 5. Temporal variation of simulated force terms defined in the equation (4) at coincident position of probe THE in the MHD frame. (a) Plasma pressure, (b) $\rho(\partial V/\partial t)$, (c) $\rho(Vg\nabla)V$, (d) plasma pressure gradient force, and (e) Lorentz force. The two vertical dashed lines indicate the time at 51 and 55 min.

2015]. Figure 4c shows the magnetic field B in the GSM coordinate. Negative B_x means that the location is in the Southern Hemisphere. The magnitude of B_y is very small being close to 0. Positive B_z means that the location is well earthward of the NENL. B_z experiences a two-step enhancement, which could be considered as the dipolarization [*Sergeev et al.*, 1993; *Baumjohann et al.*, 1999]. The first one could be regarded as dipolarization front moving earthward [*Nakamura et al.*, 2002; *Runov et al.*, 2009; *Sergeev et al.*, 2009]. In the global MHD simulation, the dipolarization continues during the expansion phase, which is consistent with previous observations [e.g., *Baumjohann et al.*, 1999]. Figure 4d shows the current density J. It is obvious that J_y is the dominant component during the interval of interest. J_y undergoes a sharp increase about 1 min after the substorm expansion onset and then begins to decrease. When the plasma pressure starts to increase at ~55 min (corresponding to the encounter of the sub HPR), the polarity of J_y turned from positive to negative. We divided the current density J into the perpendicular component $J_\perp$, and the parallel component $J_{||}$, which are shown in Figures 4e and 4f, respectively. It is found that $|J_{||}|$ is much smaller than $|J_\perp|$, and the intensification of J_y found in Figure 4d essentially comes from the perpendicular current. We further divide the perpendicular current $J_\perp$ into the inertial current (J_{in}), and the diamagnetic current (J_d). For isotropic pressure, the perpendicular current can be defined as follows

$$\begin{aligned} J_\perp &= J_{in} + J_d \\ &= \frac{B}{B^2} \times \rho \frac{dV}{dt} + \frac{B \times \nabla P}{B^2}, \end{aligned} \tag{3}$$

where ρ is the mass density. Figures 4g and 4h demonstrate J_{in} and J_d, respectively. We found two characteristics to be noted in the Y component of the current density. First, it is obvious that J_y is dominated by the diamagnetic current before ~55 min, which may result from the establishment of the main HPR. Second, the diamagnetic current is almost compensated by the inertial current after ~55 min. That implies that the inertial current is intensified, but is almost canceled by the diamagnetic current that results from the establishment of the second peak of the pressure. Because the (dawnward) inertial current is stronger than (duskward) diamagnetic current, J_y is negative (dawnward) after ~55 min.

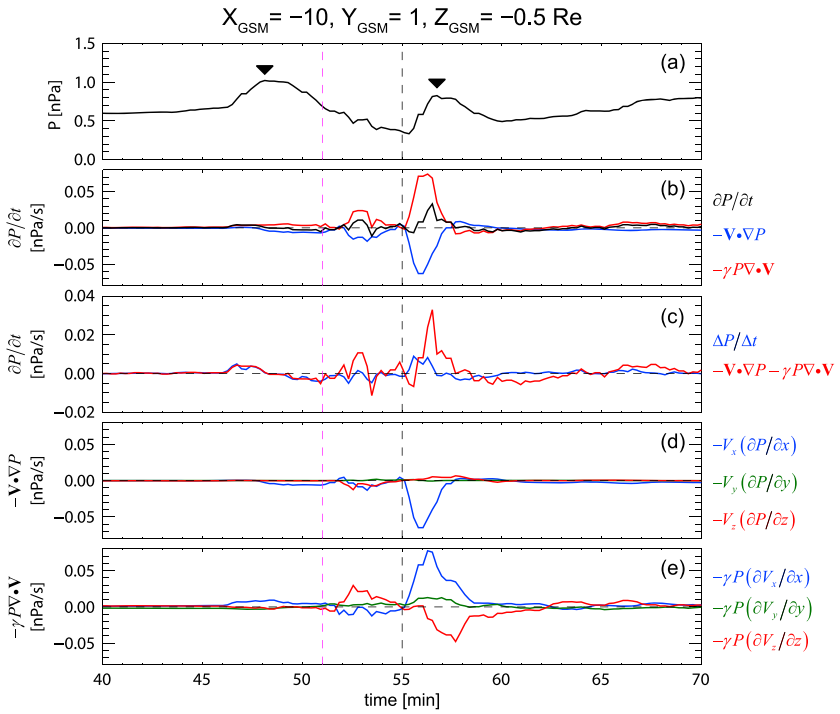

Figure 6. Temporal variation of simulated (a) plasma pressure, (b) $\partial P/\partial t$, term 1 ($-Vg\nabla P$) and term 2 ($-\gamma P\nabla gV$) on the right-hand side of the equation (5) in the black, blue, and red lines, respectively, (c) $\partial P/\partial t$ in blue line, and ($-Vg\nabla P - \gamma P\nabla gV$) in red line, (d) three subterms of the term 1, (e) three subterms of term 2. The two vertical dashed lines indicate the time at 51 and 55 min.

We calculated the force density. Figure 5 summarizes four terms of the force density given in equation (4),

$$\rho\frac{\partial V}{\partial t} + \rho(V\cdot\nabla)V = -\nabla P + J \times B. \tag{4}$$

The four terms from left to right in equation (4) are called a temporal term, a convection term, pressure gradient force term, and a Lorentz force term and shown in Figures 5b–5e, respectively. The magnitude of the temporal term is minor as compared with the convection term except near the onset (~51 min). Near the onset, the imbalance between the pressure gradient force (Figure 5d) and the Lorentz force (Figure 5e) results in the local acceleration and an increase in the earthward velocity (Figure 4b). After the onset, the plasma is accelerated earthward by the convection term (Figure 5c). In Figure 5c, it is found that in the X_{GSM} direction the convection term undergoes two different progresses. During the first interval between 51 and 55 min, the convection term is almost positive because the plasma is transported earthward by the tension force (Lorentz force) [*Tanaka et al.*, 2010] as indicated in Figure 5e. During the second interval between 55 and 59 min, it is found that the convection term is largely negative. The plasma is primarily decelerated by the pressure gradient force as well as the Lorentz force in the X_{GSM} direction. Since the temporal term is much smaller than the convection term, it can be safely said that flow braking [*Shiokawa et al.*, 1997] takes place during the second interval.

To understand the evolution of the plasma pressure, the following adiabatic equation [*Tanaka et al.*, 2010] was evaluated

$$\frac{\partial P}{\partial t} = -V\cdot\nabla P - \gamma P\nabla\cdot V, \tag{5}$$

where γ is a specific heat ratio being equal to 5/3. The first term on the right-hand side of the equation is regarded as the convection of the plasma pressure, and the second term is regarded as convergence of the plasma flow. We refer these two terms to $(\partial P/\partial t)_1$ and $(\partial P/\partial t)_2$, respectively. Figure 6 summarizes all the relevant quantities at (−10, 1, −0.5) *Re*, which is the coincident position of probe THE. In Figure 6b, $(\partial P/\partial t)_1$ and $(\partial P/\partial t)_2$ are shown in blue and red lines, respectively. The black line indicates a sum of them,

that is $(\partial P/\partial t)_1$ and $(\partial P/\partial t)_2$. A blue line in Figure 6c indicates $\Delta P/\Delta t$ that was derived from a simple differential calculation of P. A red line in Figure 6c is the same as the black line in Figure 6b. Because of unwanted numerical error in the evaluating the equation, the red line ($\partial P/\partial t$) is not identical with the blue line ($\Delta P/\Delta t$) as previously discussed by *Yao et al.* [2015]. The first term $(\partial P/\partial t)_1$ is divided into three subterms: $-V_x(\partial P/\partial x)$, $-V_y(\partial P/\partial y)$, and $-V_z(\partial P/\partial z)$, which are shown in Figure 6d. The second term $(\partial P/\partial t)_2$ is also divided into three subterms: $-\gamma P(\partial V_x/\partial x)$, $-\gamma P(\partial V_y/\partial y)$, and $-\gamma P(\partial V_z/\partial z)$, which are shown in Figure 6e. We found that the essential cause of the pressure enhancements peaking at ~48 min and ~56 min is the $-\gamma P(\partial V_x/\partial x)$ term (blue line in Figure 6e), that is the convergence of the plasma flow in the X_{GSM} direction.

3. Discussion

We have identified two ion pressure peaks taking place just before and after the substorm expansion onset in the near-Earth plasma sheet in the data from the THEMIS probes. From the multispacecraft observations, it can be said that the first peak propagates earthward, and the latter one propagates tailward. In the previous study, *Yao et al.* [2015] found the tailward propagation of the HPR just after the onset but did not identify the earthward implosion before the onset. The difference between the previous study and this study comes from the distance from the equatorial plane. In this study, the THEMIS probes were located at 0.0, 0.3 and −1.0 *Re* in Z_{GSM}, whereas in the previous study they were located at −1.9, −1.5, −1.4, and −0.9 *Re* in Z_{GSM}. The global MHD simulation also shows that two peaks of the plasma pressure appears near the equatorial plane only, which is consistent with the THEMIS observations. The distance from the equatorial plane is crucial to identify the evolution of the plasma pressure in the near-Earth plasma sheet.

We have identified in this study that the subterm $-\gamma P(\partial V_x/\partial x)$ is a dominant contributor to the plasma pressure enhancement near the equatorial plane before and after the onset. At the off-equator, the subterm $-\gamma P(\partial V_z/\partial z)$ is found to be a dominant contributor to the plasma pressure enhancement [*Yao et al.*, 2015]. As *Yao et al.* [2015] have stated, the pressure is enhanced near the equatorial plane first. The enhancement of the pressure near the equatorial plane results in the plasma flow away from the equatorial plane. Thus, V_z depends on Z, that is, $\partial V_z/\partial z < 0$, resulting in the enlargement of the $-\gamma P(\partial V_z/\partial z)$ term, that is, $\partial P/\partial t > 0$ at off-equator. In this sense, the pressure enhancement takes place in a two-step way, and we believe that we could identify the pressure enhancement caused by both the ways. In any case, it can be said that the convergence of the plasma flow (that is $-\gamma P\nabla gV$) plays an important role in enhancing the pressure before and after the onset.

In a pseudo-breakup event occurred on 22 March 2010, *Yao et al.* [2014] found that the diamagnetic current may play a major role in contributing to the cross-tail current reduction at X_{GSM}~−11 *Re*. Because the pseudo-breakup event is considered to be caused by the same physical processes as the substorm, it is plausible to make a comparison between each other. On the basis of the THEMIS data *Yao et al.* [2014] calculated the pressure gradient in the Y_{GSM} and Z_{GSM} directions, in which the probes were located at (~−11, −3, 0) *Re* and then estimated the diamagnetic current and the current derived from the Ampere's law. It is found that the simulated $\partial P/\partial z$ and J_d from the MHD simulation at the coincident position of probe THE at (−11.1, 2.3, 0.0) *Re* in this study have similar trend as that calculated by *Yao et al.* [2014]. That is, J_d increases first and then decreases, which may contribute to the current reduction. From Figure 4h we found similar variation in simulated J_d during the interval between 52 and 55 min. During this interval, the perpendicular current is dominated by the diamagnetic current, so that the current reduction is mainly contributed by the reduction of the diamagnetic current, which is consistent with the observation of *Yao et al.* [2014]. In the MHD simulation, however, the perpendicular current is further decreased, and the polarity of the perpendicular current is finally opposed by the growth of the inertial current that is a dawnward current. The difference between the result of *Yao et al.* [2014] and our result may come from the difference between the pseudo-breakup and the full-breakup. In previous studies the magnitude of the inertial current is considerably less than that of the diamagnetic current [*Birn et al.*, 1999] and is normally ignored [*Keiling et al.*, 2009; *Lui et al.*, 2010]. *Shiokawa et al.* [1997] suggested that the inertial current due to the flow braking is about 1 order of magnitude smaller than the current caused by the magnetic flux pileup, which is equal to the current derived from Ampere's law. Our simulation result shows that the magnitude of the inertial current is comparable to that of the diamagnetic current; however, the inertial current is almost canceled by the diamagnetic current that is caused by the plasma pressure enhancement. Thus, to extract the inertial current from the observation is expected to be difficult.

4. Conclusions

The major conclusions are as follows.

1. We found two peaks of the ion pressure observed by the THEMIS probes located at X_{GSM}~−11 *Re* near the equatorial plane. The first peak took place just before the substorm expansion onset, and the second one took place just after the onset. The duration of the two pressure peaks is shorter in the inner region than in the outer region. This is consistent with the V structure of the high-pressure region in the distance-time diagram, which is predicted by the global MHD simulation [*Tanaka et al*., 2010].
2. The THEMIS observations show that the *Y* component of the current density J_y shows a positive excursion near the onset. According to the MHD simulation, the increase in J_y is primarily caused by the intensification of the diamagnetic current, and the decrease in it is caused by the reduction of the diamagnetic current and intensification of the inertial current. During the latter interval, the magnitude of the inertial current is comparable to that of the diamagnetic current, but the direction is opposite. Thus, the inertial current (which points mostly dawnward) does not emerge clearly in the observational data.
3. These results may provide observational evidence of the sequence of a substorm as predicted by the MHD simulation [*Tanaka et al*., 2010]. The convergence of the plasma flow caused by the change in the force balance (state transition in the plasma sheet) plays an important role in the enhancement of the plasma pressure around the substorm expansion onset.

Acknowledgments

This study was supported by KAKENHI, a grant-in-aid for Scientific Research (B) 24340119. The authors gratefully acknowledge the research grant for Mission Research on Sustainable Humanosphere from Research Institute for Sustainable Humanosphere, Kyoto University. We acknowledge NASA contract NAS5-02099 and V. Angelopoulos for the use of data from the THEMIS mission. Specifically, C.W. Carlson and J.P. McFadden for the use of ESA data; D. Larson and R.P. Lin for the use of SST data; and K.H. Glassmeier, U. Auster, and W. Baumjohann for the use of FGM data provided under the lead of the Technical University of Braunschweig and with financial support through the German Ministry for Economy and Technology and the German Center for Aviation and Space (DLR) under contract 50 OC 0302. Data from MHD simulation are available on request (Y. Ebihara: ebihara@rish.kyoto-u.ac.jp).

Michael Liemohn thanks Yanhua Liu and another reviewer for their assistance in evaluating this paper.

References

Akasofu, S.-I. (1964), The development of the auroral substorm, *Planet. Space Sci.*, *12*, 273–282.
Angelopoulos, V. (2008), The THEMIS mission, *Space Sci. Rev.*, *141*(1–4), 5–34.
Baker, D. N., T. I. Pulkkinen, V. Angelopoulos, W. Baumjohann, and R. L. McPherron (1996), Neutral line model of substorms: Past results and present view, *J. Geophys. Res.*, *101*, 12,975–13,010, doi:10.1029/95JA03753.
Baumjohann, W., M. Hesse, S. Kokubun, T. Mukai, T. Nagai, and A. A. Petrukovich (1999), Substorm dipolarization and recovery, *J. Geophys. Res.*, *104*(A11), 24,995–25,000, doi:10.1029/1999JA900282.
Birn, J., M. Hesse, G. Haerendel, W. Baumjohann, and K. Shiokawa (1999), Flow braking and the substorm current wedge, *J. Geophys. Res.*, *104*(A9), 19,895–19,903, doi:10.1029/1999JA900173.
Ebihara, Y., and T. Tanaka (2013), Fundamental properties of substorm time energetic electrons in the inner magnetosphere, *J. Geophys. Res. Space Physics*, *118*, 1589–1603, doi:10.1002/jgra.50115.
Gjerloev, J. W. (2012), The SuperMAG data processing technique, *J. Geophys. Res.*, *117*, A09213, doi:10.1029/2012JA017683.
Keiling, A., et al. (2009), Substorm current wedge driven by plasma flow vortices: THEMIS observations, *J. Geophys. Res.*, *114*, A00C22, doi:10.1029/2009JA014114.
Lui, A. T. Y. (1996), Current disruption in the Earth's magnetosphere: Observations and models, *J. Geophys. Res.*, *101*(A6), 13,067–13,088, doi:10.1029/96JA00079.
Lui, A. T. Y. (2011), Reduction of the cross-tail current during near-Earth dipolarization with multisatellite observations, *J. Geophys. Res.*, *116*, A12239, doi:10.1029/2011JA017107.
Lui, A. T. Y., E. Spanswick, E. F. Donovan, J. Liang, W. W. Liu, O. LeContel, and Q.-G. Zong (2010), A transient narrow poleward extrusion from the diffuse aurora and the concurrent magnetotail activity, *J. Geophys. Res.*, *115*, A10210, doi:10.1029/2010JA015449.
Machida, S., Y. Miyashita, A. Ieda, M. Nosé, V. Angelopoulos, and J. P. McFadden (2014), Statistical visualization of the Earth's magnetotail and the implied mechanism of substorm triggering based on superposed-epoch analysis of THEMIS data, *Ann. Geophys.*, *32*, 99–111, doi:10.5194/angeo-32-99-2014.
McFadden, J. P., C. W. Carlson, D. Larson, M. Ludlam, R. Abiad, B. Elliott, P. Turin, M. Marckwordt, and V. Angelopoulos (2008), The THEMIS ESA Plasma Instrument and In-flight Calibration, *Space Sci. Rev.*, *141*(1–4), 277–302.
Nakamura, R., et al. (2002), Motion of the dipolarization front during a flow burst event observed by Cluster, *Geophys. Res. Lett.*, *29*(20), 1942, doi:10.1029/2002GL015763.
Pu, Z. Y., et al. (1999), Ballooning instability in the presence of a plasma flow: A synthesis of tail reconnection and current disruption models for the initiation of substorms, *J. Geophys. Res.*, *104*(A5), 10,235–10,248, doi:10.1029/1998JA900104.
Runov, A., V. Angelopoulos, M. I. Sitnov, V. A. Sergeev, J. Bonnell, J. P. McFadden, D. Larson, K.-H. Glassmeier, and U. Auster (2009), THEMIS observations of an earthward-propagating dipolarization front, *Geophys. Res. Lett.*, *36*, L14106, doi:10.1029/2009GL038980.
Sergeev, V., V. Angelopoulos, S. Apatenkov, J. Bonnell, R. Ergun, R. Nakamura, J. McFadden, D. Larson, and A. Runov (2009), Kinetic structure of the sharp injection/dipolarization front in the flow-braking region, *Geophys. Res. Lett.*, *36*, L21105, doi:10.1029/2009GL040658.
Sergeev, V. A., D. G. Mitchell, C. T. Russell, and D. J. Williams (1993), Structure of the tail plasma/current sheet at ~11 RE and its changes in the course of a substorm, *J. Geophys. Res.*, *98*(A10), 17,345–17,365, doi:10.1029/93JA01151.
Shiokawa, K., W. Baumjohann, and G. Haerendel (1997), Braking of high-speed flows in the near-Earth tail, *Geophys. Res. Lett.*, *24*, 1179–1182, doi:10.1029/97GL01062.
Tanaka, T., A. Nakamizo, A. Yoshikawa, S. Fujita, H. Shinagawa, H. Shimazu, T. Kikuchi, and K. K. Hashimoto (2010), Substorm convection and current system deduced from the global simulation, *J. Geophys. Res.*, *115*, A05220, doi:10.1029/2009JA014676.
Tsyganenko, N. A. (1989), A magnetospheric magnetic field model with a warped tail current sheet, *Planet. Space Sci.*, *37*(1), 5–20.
Yao, Y., Y. Ebihara, and T. Tanaka (2015), Sudden pressure enhancement and tailward retreat in the near-Earth plasma sheet: THEMIS observation and MHD simulation, *J. Geophys. Res. Space Physics*, *120*, 201–211, doi:10.1002/2014JA020482.
Yao, Z. H., et al. (2014), Current reduction in a pseudo-breakup event: THEMIS observations, *J. Geophys. Res. Space Physics*, *119*, 8178–8187, doi:10.1002/2014JA020186.

AGU Journal of Geophysical Research: Space Physics 10.1002/2015JA021187

Erratum

In the originally published version of this article, equations (4) and (5) each contain instances where the dot-product "·" should have appeared instead of the letter "g". The error has since been corrected, and this version may be considered the authoritative version of record.